Springer

KSME

Journal of Mechanical Science and Technology 24 (7) (2010) 1389~1400
www.springerlink.com/content/1738-494x
DOI 10.1007/s12206-010-0413-5

Flow uniformity in a multi-intake pump sump model †

Jong-Woong Choi[1], Young-Do Choi[2] , Chang-Goo Kim[1] and Young-Ho Lee[3,*]

[1]*Department of Mechanical Engineering, Graduate School, Korea Maritime University, Busan, 606-791, Korea*
[2]*Department of Mechanical Engineering, Mokpo National University, Jeonnam, 534-729, Korea*
[3]*Division of Mechanical Engineering and Information, Korea Maritime University, Busan, 606-791, Korea*

(Manuscript Received June 1, 2009; Revised February 23, 2010; Accepted March 2, 2010)

Abstract

The head-capacity curves for pumps developed by the pump manufacturer are based on tests of a single pump operation in a semi-infinite basin with no close walls or floors and with no stray currents. Therefore, flow into the pump intake is with no vortices or swirling. However, pump station designers relying on these curves to define the operating conditions for the pump selected sometimes experience reductions of capacity and efficiency, as well as the increase of vibration and additional noise, which are caused by free air mixed with the pump inlet flow. Therefore, sump model test is necessary in order to examine the flow structure around pump intake. In this study, flow uniformity according to the flow distribution in the pump intake channel is examined to find out the cause of vortex occurrence in detail. A multi-intake pump sump model with 7 pump intakes and a single-intake pump sump model are adopted for the investigation. Furthermore, effectiveness of anti-submerged vortex device (AVD) for the suppression of the vortex occurrence in a single pump intake, as well as in a multi-intake pump sump model has been examined by the methods of experiment and numerical analysis. The results show that most high value of flow uniformity is found at the inlet of pump intakes #3 and 5 in the multi-intake pump sump with 7 pump intakes. Therefore, when the pump station is designed, the flow patterns at the upstream region of pump intake inlet in the forebay diffusing area should be to consider in detail because the unbalanced flow at the channel inlet region gives considerable influence on the vortex occurrence around bell-mouth. Strong submerged vortex can be successfully suppressed by AVD installation on the bottom of pump intake channel just below the bell mouth.

Keywords: Pump sump model; Free-surface vortex; Submerged vortex; Anti-submerged vortex device; Flow uniformity

1. Introduction

Generally, performance curves for pumps developed by the pump manufacturer are based on tests of a single pump operating in a semi-infinite basin with no close walls or floors and with no stray currents. Therefore, flow into the pump intake is with no vortices or swirling. However, pump station designers relying on these curves to define the operating conditions for the pump selected sometimes meet the reductions of capacity and efficiency, as well as the increase of vibration and additional noise, which are caused by free air mixed with the pump inlet flow. Therefore, sump model test is necessary in order to examine the flow structure around pump intake.

As related studies for the flow into the pump intake, many research results can be found in the open literature and some representative research results are summarized as followings.

Padmanabhan and Hecker [1] have defined vortex shapes occurring around the pump intake and the vortex shapes are classified by Froude number for the reduced scale ratio of the pump sump model. Rajendran et al. [2] have made a numerical analysis for the 3-D turbulent flow in a pump sump model including pump intake, and numerical results are compared and analyzed with that of experiment. Kamemoto et al. [3] have found that essential characteristics of vortex formation observed in the two models, which have different sizes but same configuration, are completely similar each other although the scale of the inner diameter of the smaller scale model is less than the lower limit value of 100mm. Nagahara et al. [4] have conducted PIV experiment and CFD analysis for the flow structure by uneven flow velocity around pump intake in a pump sump model. Lee [5] has suggested a design guideline for the shape of pump sump by model test and CFD analysis.

Moreover, Turbomachinery Society of Japan [6] has revised the standard of pump sump model test and the revised standard examined the possibility of numerical analysis for the prediction of the flow in the sump model using several commercial and in-house CFD codes.

† This paper was recommended for publication in revised form by Associate Editor Yang Na

*Corresponding author. Tel.: +82 51 410 4293, Fax: +82 51 403 0381
E-mail address: lyh@hhu.ac.kr

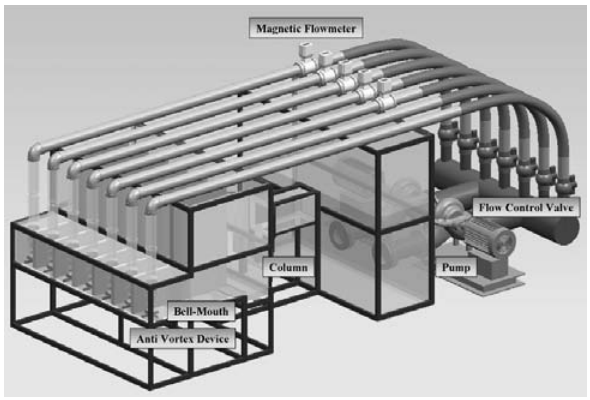

Fig. 1. Experimental setup of multi-intake pump sump model.

The purpose of this study is to examine the flow uniformity according to the flow distribution in each pump intake channel for a multi-intake pump sump model with 7 pump intakes. Furthermore, effectiveness of anti-submerged vortex device (AVD) for the suppression of the vortex occurrence in a single-intake pump sump model, as well as in a multi-intake pump sump model has been examined by the methods of experiment and numerical analysis.

2. Experimental and Numerical Methods

2.1 Experimental setup

2.1.1 Test pump sump model layout

Fig. 1 shows pump sump model test loop which is designed according to the prototype sump layout by scale ratio of 1:10. All dimensions are precisely accurate within 1mm order of allowance except bell mouth which is manufactured by NC machine with less than 0.1mm allowance. Seven flow control valves afford pump combination operation. The valve type is ball valve. Five magnetic flowmeter transmitters are installed at the top pipelines. The electro-magnetic flow meters have sufficient straight pipelines before the flowmeter and are earthed to power supply terminal for normal signal production. All flow meters are calibrated before installation. The final suction pipelines are replaced by flexible composite material vinyl pipes of 150mm diameter because the original PVC 90 degree elbows causes severe flow resistance owing to their mal-functioned shape.

Two doubled-suction centrifugal pumps (each flow rate 900m^3/hr, head 8m, 55kW) are installed for the circulating water supply within the sump model test. Screen mesh installed at the entrance of pump intake bay gives reduction of flow fluctuation. Pump front bay wall is made of transparent plate for vortex observation and photo recording (refer to Figs. 7 and 8).

Fig. 2 shows the plane view of test pump sump model. The numbering of model pump intakes is given from left #1 to right #7 in sequence. The width of entire pump bay is 3,220mm and fore bay expanding length is 1,148mm with 1,000mm straight passage from intake channel. Intake channel

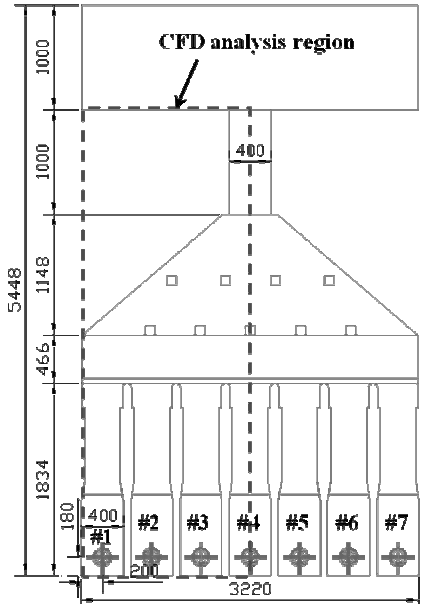

Fig. 2. Plane view of pump sump model and CFD analysis region.

width is 3,220mm and its flow direction length is 1,000mm. The width of each pump intake channel is 400mm at bell mouth side. The centers of bell-mouth inlet in each pump intake channel are located at 200mm, 180mm and 100mm from side wall, rear wall and bottom of each pump intake channel in the pump sump model, respectively.

For the pump intake channel length of 1,834mm, the height of model pump bay in the region near pump intake pipe, which has the length of 780 in flow direction, is fixed to 600mm and the upper side of each pump intake is covered in order prevent air suction from free surface in the pump intake. However, the height of the other region in the pump intake channel is fixed to 1,690mm and the channel upper side is open to air. The flow obstacles of 90mm×90mm square bar shape installed in expanding forebay are arranged to attenuate flow fluctuation occurring by the abrupt expansion of the flow passage at the upstream region.

Clean tap water is used as working fluid. Water and air temperatures during the experiment in the laboratory are 24°C and 16°C, respectively.

2.1.2 Bell-mouth and anti-submerged vortex device (ADV)

Fig. 3 shows cross-sectional view and detailed dimensions of a bell-mouth and an anti-submerged vortex device.

The bell-mouth is installed at the inlet of intake pipe. The diameter of bell mouth model inlet is determined to 150mm considering the scale ratio of 1:10 for all pump intakes in the pump sump model. Careful NC manufacturing technique is given for the precise dimension of bell mouth configuration. The anti-submerged vortex device, which has the cross-shaped rectangular bar with 99 degree taped end, shall be attached at the bottom of pump intake channel just below the bell mouth. Cross bar bottom width is 24mm and upper width is 12mm.

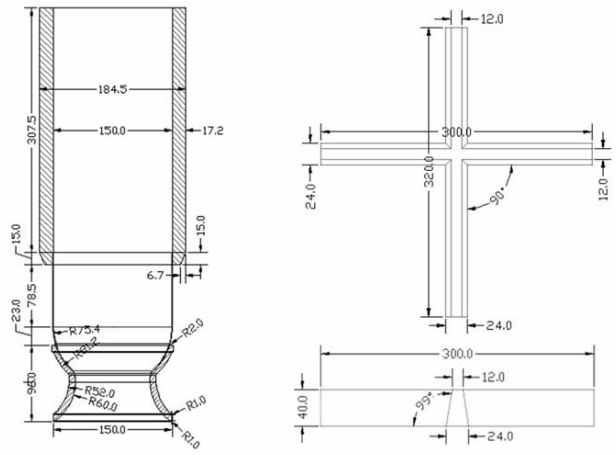

(a) Bell-mouth (b) ADV

Fig. 3. Bell-mouth and anti-submerged vortex device (AVD).

Its height is 40mm.

2.1.3 Model test operation

Two main circulating pumps suck flows from model bell mouths and then discharges sucked flows into lower water tank of the intake channel. Pump operation condition of 10 combinations for both free and submerged vortex tests is selected considering the flow fields possible in the sump. The 10 combinations of pump operation include single, triple and 4, 5 or full seven pumps selection.

Flow conditions are both twice Froude No. for free-surface vortex test and equal velocity for submerged vortex test (refer to following subsection 2.2 for the flow conditions). Same water level of 563mm is kept for both flow conditions. The flow rates of the model pump are 121m^3/hr for twice Froude No. and 192m^3/hr for equal velocity conditions.

2.1.4 Uncertainty analysis

The uncertainty analysis for flow rate is based on the method of Abernethy et al. [7]. The total uncertainty (U) of the variables can be found by combining systematic and random errors as : $U=[B^2+(tS_{\overline{X}})^2]^{1/2}$, where B is the systematic uncertainty, $S_{\overline{X}}$ is the standard deviation of the mean, and the degree of freedom t is determined to 2 for a 95% confidence level (for a sample size greater than 50). The systematic uncertainty B is estimated based on the calibration data and previous test experience, and the standard deviation of the mean $S_{\overline{X}}$ is computed from the raw test data. Measurement uncertainty for flow rate is estimated to be $Q=\pm 1.39$ percent when all 7 pump intakes in the multi-intake pump sump model are operated by keeping the incoming velocity of 3m/s into the bell-mouth inlet.

2.2 Principle of similarity

As an experimental criterion of vortex occurrence estimation, HI standard [8] is adopted. The adopted principle of similarity between model and prototype is as followings.

2.2.1 Same Froude-number velocity (observing free-surface flow)

Froude No. (F_r) is kept the same for the model and prototype. The Froude-number is by the ratio of gravitational and inertial forces. The condition of free surface is fundamentally governed by the Froude No. as defined in Eq. (1).

$$F_r=\frac{V_m}{\sqrt{gL_m}}=\frac{V_p}{\sqrt{gL_p}} \tag{1}$$

In this test, Eq. (2) is obtained.

$$V_m=V_p\times\left(\frac{L_m}{L_p}\right)^{0.5}=\left(\frac{1}{10}\right)^{0.5}\times V_p$$

or

$$Q_m=Q_p\times\left(\frac{L_m}{L_p}\right)^{0.5}=\left(\frac{1}{10}\right)^{0.5}\times Q_p \tag{2}$$

2.2.2 Froude scaled flow (twice Froude No.)

In order to observe free-surface vortex, the scaled flow model test is conducted with keeping the submergence at the geometrically scaled values as Eq. (3).

$$V_m=2.0\times V_p\times\left(\frac{L_m}{L_p}\right)^{0.5}=2.0\times\left(\frac{1}{10}\right)^{0.5}\times V_p$$

or

$$Q_m=2.0\times Q_p\times\left(\frac{L_m}{L_p}\right)^{2.5}=2.0\times\left(\frac{1}{10}\right)^{2.5}\times Q_p \tag{3}$$

2.2.3 Equal velocity (examining submerged vortex)

Development of submerged vortex is considered owing to flow velocity around a pump sump bell-mouth. Therefore, the submerged vortex test requires flow velocity of both actual and model pump sumps equal. This is applied to examine subsurface vortex as well as submerged vortex with following Eq. (4) between model and prototype.

$$V_m=V_p$$

and

$$Q_m=Q_p\times\left(\frac{L_m}{L_p}\right)^{2.0} \tag{4}$$

2.2.4 Relation between model and prototype

Relationship between relevant quantities for the model and prototype adopted in this study is shown in the following Table 1.

Table 1. Relationship between model and prototype.

Parameter	Froude No.	Scaled Froude No.	Equal velocity
Length	1 : 10	1 : 10	1 : 10
Velocity	$1 : 10^{0.5}$ = 1 : 3.16	$1: 0.5\times10^{0.5}$ = 1 : 1.58	$1 : 10^{0}$ = 1 : 1
Flow rate	$1 : 10^{2.5}$ = 1 : 316.2	$1: 0.5\times10^{2.5}$ = 1 : 158.1	$1 : 10^{2.0}$ = 1 : 100
Time	$1 : 10^{0.5}$ = 1 : 3.16	$1: 0.5\times10^{0.5}$ = 1 : 1.58	1 : 10

2.3 Numerical methods

2.3.1 Numerical conditions and grids

As the free-surface vortex test shows no vortex occurrence under the twice Froude No. condition, present CFD analysis is conducted only under the calculation condition of equal velocity.

Fig. 2 shows the plane view of pump sump model and the area enclosed with dotted line is computational domain. Test pump sump model has 7 pump intakes. However, for the calculation of the flow field in the pump sump model, only the half area of the model flow field is analyzed because the pump sump model consists of symmetric configuration, and thus reduction of the calculation load and time is possible by the calculation for the half flow field area.

Using a 3-D modeling data for the multi-intake pump sump model, a fine hexa-hedral computational grid for steady state calculation is embodied as shown in Fig. 4. For the multi-intake pump sump model, total node number of the computational grid is determined to 3.3×10^6 taking computer calculation performance into consideration. Moreover, numerical grid for a single-intake pump sump model, which has the same dimensions as the pump intake forebay in the multi-intake pump sump model, is also embodied independently with the same grid number of one pump intake forebay in the multi-intake pump sump model.

For the processing of numerical simulation, a commercial CFD code of ANSYS CFX [9] is adopted. As boundary conditions for the steady state calculation, zero pressure gradient at the inlet and averaged velocity of 3m/s at the bell-mouth inlet are applied considering the equal velocity flow condition. Water level is kept to 563mm.

As the wall conditions, free-slip condition is applied to the upper side of pump sump model passage from the end of expanding passage region to the first half region of pump intake bay near the inlet of the pump intake channel. No-slip condition is applied to side and upper walls both near calculation domain inlet and at the second half region of pump intake channel near bell-mouth. Symmetry condition is applied to the center wall as shown in Fig. 4.

SST (Shear Stress Transport) turbulence model is used to realize the complicated vortex flow around the pump sump in detail. SST model is two equation turbulence model by Menter et al. [10]. It is a blend of Wilcox's original k-ω model with k-ε model. It has been found to more accurately predict flow separation by accounting for the transport of turbulent shear stress.

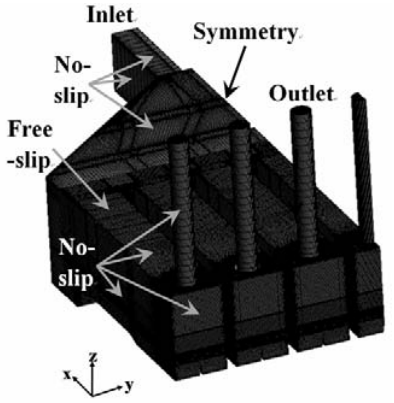

(a) Multi-intake pump sump model

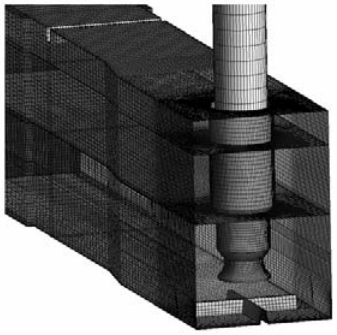

(b) Single-intake pump sump model

Fig. 4. Computational hexa-hedral grid and wall conditions.

In order to apply SST model to a numerical flow filed successfully, y+ value should be determined below y+ ≤ 2 [9]. CFX solver adopts two turbulence models according to sub-layer value. : k-ω model is used below the sub-layer value of 11.067 but k-ε model is also adopted over the sub-layer value. Moreover, when k-ε model is adopted, scalable wall function is applied.

However, in order to solve the problem of excessive grid number requirement for the whole flow field of test model, TSJ model (Fig. 5) is adopted for the validation test. And thus, the validation result, especially for the y+ value, is applied to the present numerical flow field. Present multi-intake pump sump model adopts the y+ value range of 0.2~200.

2.3.2 Validation test of present CFD analysis method

In order to acquire the reliability of present CFD analysis method, bench marking simulation for the determined shape of a single pump intake is performed. The benchmarking pump intake model is given by Turbomachinery Society of Japan (TSJ) [6] for the purpose of performance evaluation of commercial and in-house CFD codes for pump sump.

Fig. 5 shows the TSJ pump sump model for benchmarking simulation. The test model is embodied by 3-D modeling using CAD software. After calculation grid is produced using the CAD data, steady state calculation is conducted for the test

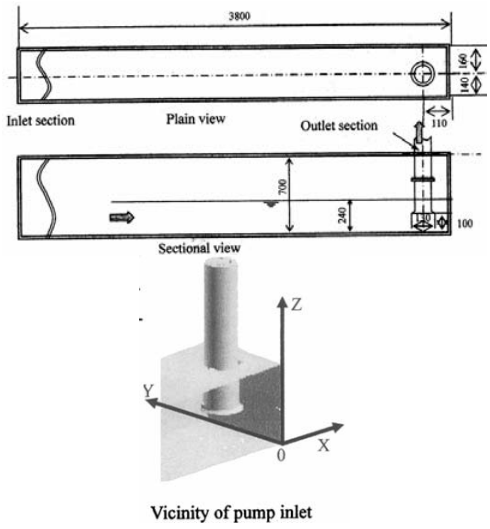

Fig. 5. Benchmarking pump sump model for CFD analysis (for air-entrained vortices) [6].

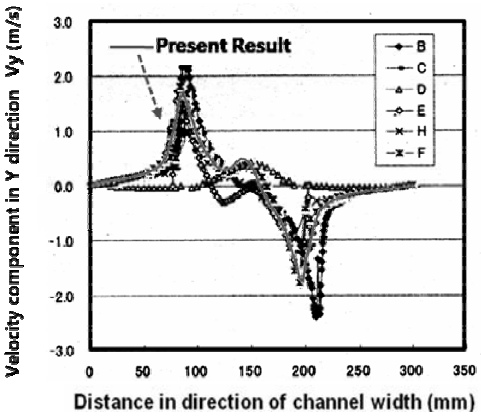

(a) Y direction

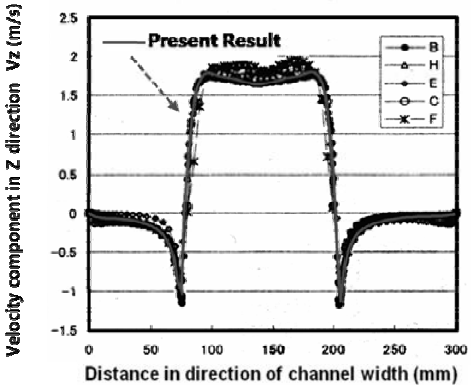

(b) Z direction

Fig. 6. Comparison of present CFD result with the benchmark CFD results.

model using the CFD analysis method adopted in this study.

The calculated results for validation test reveal that velocity component distributions in Y and Z-directions of present CFD analysis method agree well with the results by other CFD codes as shown in Fig. 6. Especially, in case of the velocity component distribution to Y-direction, eccentrical whirling flow according to the eccentricity of the intake pipe location is found as shown in Fig. 6(a). In the velocity component distribution to Z-direction, present CFD code expresses the flow behavior well that the velocity component around the inlet of the intake pipe is relatively low, but the velocity component becomes accelerated considerably after the flow enters the bell-mouth inlet as shown in Fig. 6(b).

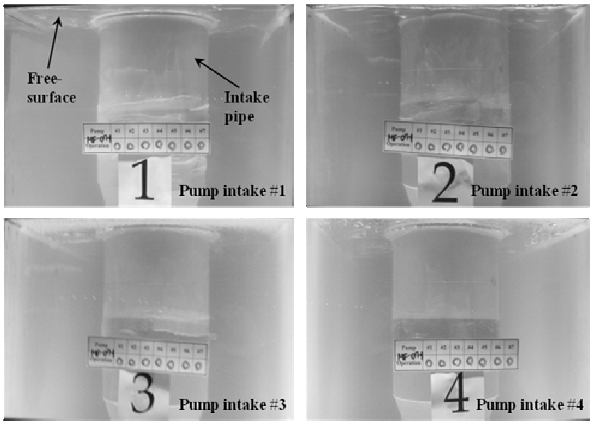

Fig. 7. Observation of free-surface vortex in the multi-pump intake (twice Froude number condition).

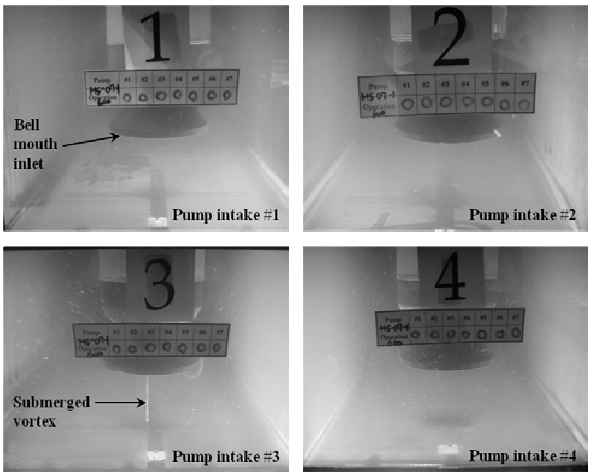

Fig. 8. Occurrence of submerged vortex in the multi-pump intake (Without AVD, equal velocity condition).

3. Results and discussions

3.1 Observation of vortex occurrence in a multi-intake pump sump model

3.1.1 Observation of free-surface vortex and submerged vortex

In order to observe free-surface vortex and submerged vortex, flow conditions of the twice Froude No. and equal velocity are adjusted according to HI standard [8], respectively.

Fig. 7 shows an example of free-surface vortex observation in the case of all pump intake operation in the multi-intake pump sump model. The pictures are captured just under the

Table 2. Observation of vortex occurrence by multi-intake pump sump model test.

Combination of pump operation (Operating pump intake No.)	Total flow rate (m^3/hr)		Pump intake No.		
	Twice Froude number	Equal velocity	Free-surface vortex occurrence	Submerged vortex occurrence (Pump intake No.)	
				Without ADV	With ADV
#1	121×1	192×1	No free-surface vortex occurrence	×	No submerged vortex occurrence
#3	121×1	192×1		×	
#5	121×1	192×1		#5	
#1+#3+#4	121×3	192×3		#3	
#1+#3+#5	121×3	192×3		#3, #5	
#2+#3+#4	121×3	192×3		#2*, #3	
#1+#2+#3+#4	121×4	192×4		#2*, #3	
#1+#2+#3+#5	121×4	192×4		#2*, #3, #5	
#1+#2+#3+ #4+#5	121×5	192×5		#1*, #2*, #3, #4*, #5	
#1+#2+#3+#4 +#5+#6+#7	121×7	192×7		#1*, #2*, #3, #5, #6*, #7*	

*: vortex occurs intermittently

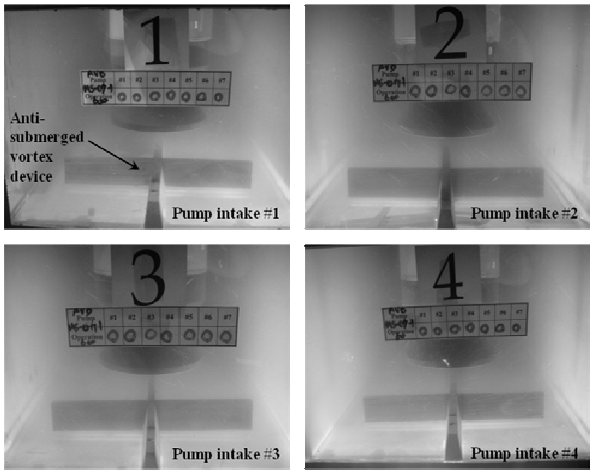

Fig. 9. Suppression of submerged vortex in the multi-pump intake by anti-submerged vortex device (With AVD, equal velocity condition).

free surface and around the intake pipes. Typically, all pump intake operation gives most severe condition leading to the possible occurrence of vortex. In the case of free-surface vortex observation by twice Froude No., no vortex at all pump operation condition is detected due to sufficient submerged depth.

However, in case of submerged vortex observation by equal velocity condition, Fig. 8 shows considerable occurrence of the submerged vortex with strong intensity in pump intakes #3 when all pump intakes are operated. The observed submerged vortex is defined as B-3 air-core bubble vortex according to the HI standard [8]), and intermittent submerged vortex occurrence is also observed in the other pump intakes.

Table 2 shows the observation results of vortex occurrence in the multi-intake pump sump model.

3.1.2 Suppression of submerged vortex by ADV

From the test of submerged vortex observation by all pump intake operation, strong B-3 air-core bubble vortex and intermittent air bubble vortex are always visible at equal velocity flow condition. To countermeasure this vortex, a cross-shaped bar AVD is installed at the bottom of pump bay just below the bell mouth of main pump, and its result is successful disappearance of generated vortex as shown in Fig. 9. Moreover, the experimental results show satisfactory removal of the submerged vortex by the AVD in all flow conditions as shown in Table 2.

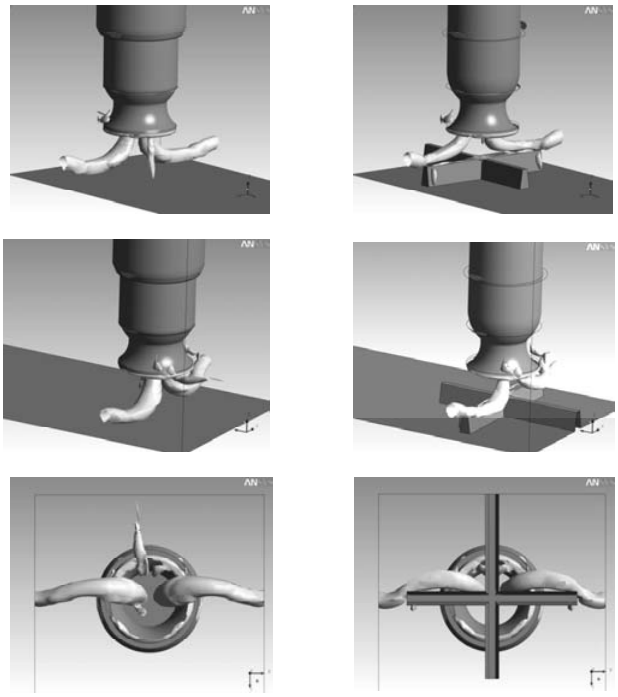

(a) Without AVD (b) With AVD

Fig. 10. Vortex core region of single intake sump.

3.2 Flow analysis of a single-intake pump sump model

3.2.1 Vortex core region in a single intake sump

Before the calculation of whole flow field in the multi-intake pump sump model, a single pump sump, which has the same dimensions as those of each pump intake forebay in the multi-intake pump sump, is adopted to examine the effect of AVD on the suppression of submerged vortex.

Fig. 10 shows the calculation results of vortex core region by the cases of both without and with the AVD when the incoming velocity is set to 3m/s at the inlet of the bell-mouth. The vertex core region in this study is revealed by iso-surface of swirling strength which represents the strength of the local swirling motion.

Fig. 10(a) shows the calculated result in case of no AVD and the vortex structures occurring from the rear wall, side wall and bottom can be observed. Fig. 10(b) shows the case of AVD installation at the bottom of the pump sump and the vortex core region becomes considerably decreased in the vicinity of the bottom and rear wall. Moreover, vortex core region occurring from the side wall is also reduced.

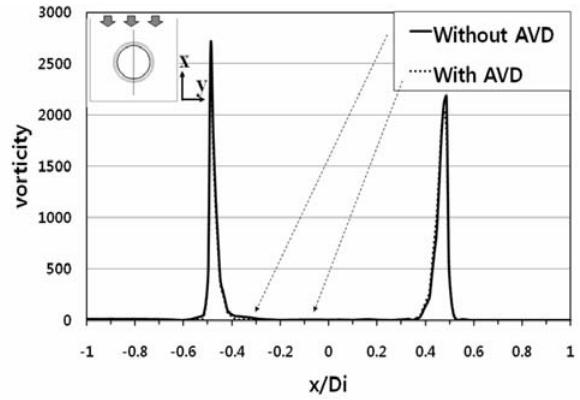

(a) H=100 mm

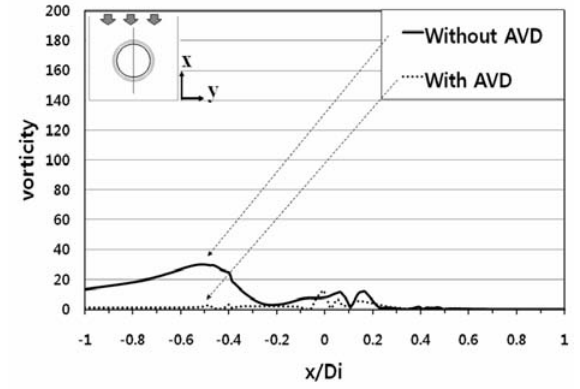

(b) H=80 mm

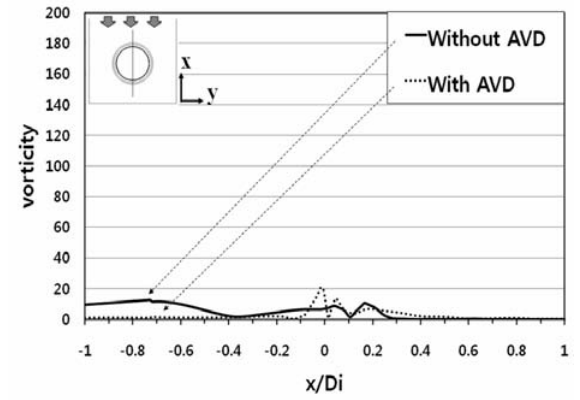

(c) H=60 mm

Fig. 11. Vorticity in flow direction.

3.2.2 Reduction of vorticity by the effect of AVD

In order to examine the vortex intensity around the intake pipe quantitatively, vorticity is plotted in Figs. 11 and 12. Moreover, sampling locations of the data are shown in the left-upper side of each graph.

Fig. 11 shows vorticity distribution in flow direction at each height of H=100mm, 80mm and 60mm. Ordinate of the graphs indicates the vorticity value and abscissa means the distance ratio from the center of the bell-mouth. When the AVD is installed on the bottom of the pump intake, reduction of vorticity in the vicinity of rear wall (x/D_i=-1) is clearly perceptible in comparison with the case by no AVD.

Table 3. Maximum & mean vorticity values of a single-sump.

Distance from bottom wall in the pump sump model		Maximum and mean vorticity values	
		without ADV	with ADV
Channel width direction	60mm	75.1 (23.4)	33.2 (16.9)
	80mm	120.7 (24.8)	27.9 (6.3)
	100mm	2240.2 {199.2} (132.8)	2394.2 {22.4} (107.6)
Flow direction	60mm	12.8 (4.7)	20.8 (2.4)
	80mm	30.2 (9.2)	12.8 (1.6)
	100mm	2683.4 (102.7)	2416.9 (95.8)

* (): mean vorticity value, **{ }:Second peak value

At the water depth of H=100mm, which is the same height of bell mouth inlet, two predominant vorticity value regions are found at the same radius of bell mouth inlet wall regardless of AVD installation. The result means that high vorticity flow enters into the bell mouth through the annular region in the vicinity of bell mouth inlet wall. As the water depth decreases to H=80mm and 60mm, almost vorticity disappears except for the region at the bell mouth center when AVD is installed. However, when AVD is installed, vorticity still remains at the left half side of the flow channel and disappears gradually as the water depth decreases.

Fig. 12 shows vorticity in direction of channel width around the center of bell-mouth. In case of no AVD, vorticity in direction of channel width changes largely symmetrically by the locations and the value is reduced as the height H is lowered. In contrast to the results by no AVD condition, when the AVD is installed, relatively small change of the vorticity is found in direction of channel width because the vortex occurring from the bottom of the pump intake is suppressed by the AVD. Moreover, the vorticity value in direction of channel width by AVD installation shows relatively very small in comparison with that by no AVD.

In addition, maximum vorticity value in flow direction (Fig. 11) is lower than that in direction of channel width (Fig. 12) by both no AVD and AVD installation. This result implies that the vortex intensity in the vicinity of side walls is higher than those both near rear wall and near the upstream region of the bell mouth.

For the more detailed comparison of the vorticity change by the installation of AVD, both of the maximum and mean values of vorticity are summarized in Table 3. When the vertical height from bottom wall of the pump intake is located at H=100mm, maximum value of vorticity shows apparently higher than those at the other heights. The high vortex value at the height of H=100mm is resulted from the strong vortex region at the tip of the bell-mouth.

Mean vorticity values in case of AVD installation at each

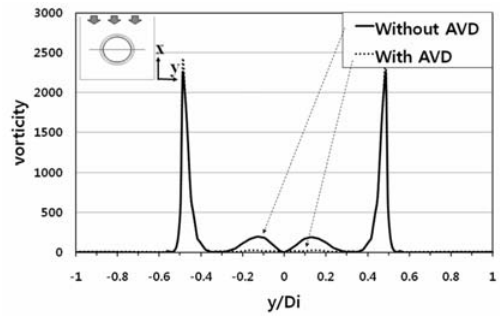

(a) H =100 mm

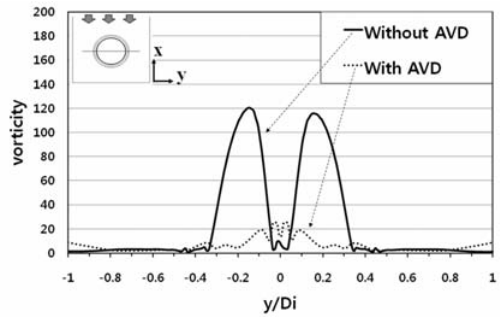

(b) H =80 mm

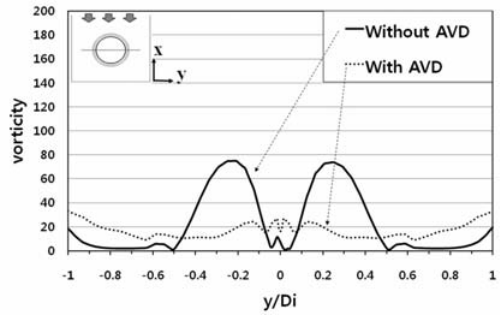

(c) H =60 mm

Fig. 12. Vorticity in direction of channel width.

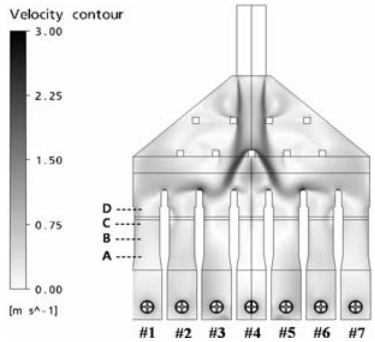

(a) H=100mm

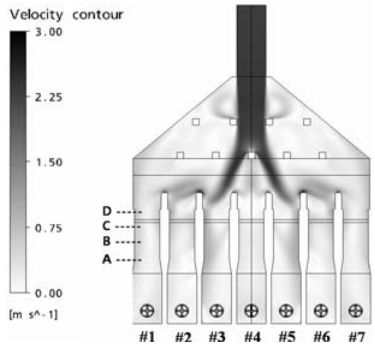

(b) H=300mm

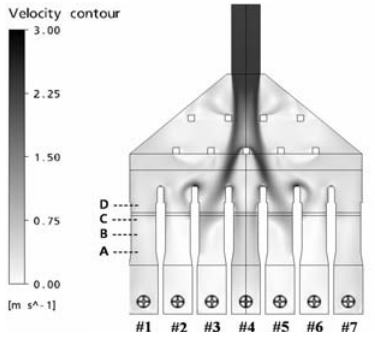

(c) H=500mm

Fig. 13. Velocity contour in the pump sump model (with AVD).

distance from the bottom wall indicate much lower than those in case of no AVD both in flow direction and channel width direction. Moreover, when the vortex values are compared between the channel width direction and flow direction, vorticity in direction of channel width shows higher value than that in flow direction. This quantitative vorticity data proves relatively strong vortex intensity at the side walls of the pump sump model.

3.3 Flow analysis of a multi-intake pump sump

3.3.1 Flow patterns in a multi-intake pump sump model

As explained in the former section, only half region of flow field in the multi-intake pump sump model is adopted for the calculation because the flow field in the multi-intake pump sump model consists of symmetric configurations.

Fig. 13 shows incoming velocity contours on the planes located at the heights of H=100mm, 300mm and 500mm from the bottom wall (H=0) of the pump sump model. Even though only the half region of the flow field is calculated, another half region is also shown together by symmetric flow pattern in the total flow field.

Incoming flow into the inlet of pump intake channel shows various flow patterns by the channel location. Especially, pump intake #3 and #5 shows most drastic variation of the velocity distribution at each height of the velocity contour plane.

Table 4 shows the approaching mean velocities in flow direction on the cross-sectional planes at the marked points of A (910mm), B (1100mm), C (1300mm) and D (15020mm) in Fig. 13. Even though the points are located relatively near the pump intake channel inlet, mean velocities at the points are almost equal regardless of the point locations and sump channel number. This result is reasonable because the suction flow rates at each intake pipe are equal.

Moreover, velocity profiles in flow direction are shown in Fig. 14 to examine the velocity variation by the channel height

Table 4. Approaching mean velocity into bell mouth inlet

(Unit : m/s)

	Approaching mean velocity			
	Sump 1	Sump 2	Sump 3	Sump 4
910mm (A)	0.258	0.259	0.259	0.252
1100mm (B)	0.259	0.259	0.259	0.253
1300mm (C)	0.259	0.259	0.259	0.266
1500mm (D)	0.259	0.259	0.259	0.262

(H=100mm, 300mm and 500mm), as well as by the intake channel number accurately. The analyzed result shows that velocity profile at the pump intake #3 shows most asymmetric to the cha2nnel passage among the velocity profiles in the pump intakes #1 to #4 on the three heights of the plane.

It is clear that the asymmetric flow pattern in the pump intake #3 is resulted from the unbalanced approaching velocity distribution at the inlet of pump intake as confirmed in Fig. 13. Therefore, one of the most important factors for the pump station design is to consider the flow patterns at the upstream region of pump intake inlet in the forebay diffusing area. The large expanding angle at the forebay diffusing area may cause unstable fluctuating flow supply to pump intake channels. Especially, pump intake channels #3 and #5 are susceptible to occurrence of strong submerged vortex, even from the present result by CFD analysis.

3.3.2 Vortex core region in a multi-intake pump sump model

Fig. 15 shows the vortex core region occurring around the intake pipes #1 to #4 in the pump sump model when AVD is installed. It is obvious that the vortex patterns occurring in each pump intake are different each other. Especially, vortex core region in the pump intake # 3 shows wider spatial area of vortex distribution than those in the other pump intakes. Therefore, it is clear from the result that the strong submerged vortex occurred in the pump intakes #3 and #5 in case of all pump intakes operation is caused by the severe non-uniform approaching flow which generate strong vorticity around the bell-mouth inlet region.

3.3.3 Vorticity distribution around the bell-mouth inlet in multi-intake pump sump

For the purpose of examining the cause of submerged vortex occurrence in detail, quantitative value of vorticity distribution around the bell-mouth inlet is investigated when ADV is installed.

In order to examine the vorticity at each position around the bell-mouth, vorticity distributions both in flow direction and channel width direction are shown in Figs. 16 and 17. When the values of vorticity around the bell-mouth in the multi-intake pump sump model (Figs. 16 and 17) are compared with those in the single-intake pump sump model (Figs. 11 and 12), on the whole, the multi-intake pump sump model reveals relatively higher values of vorticity than those of the single-intake pump sump model.

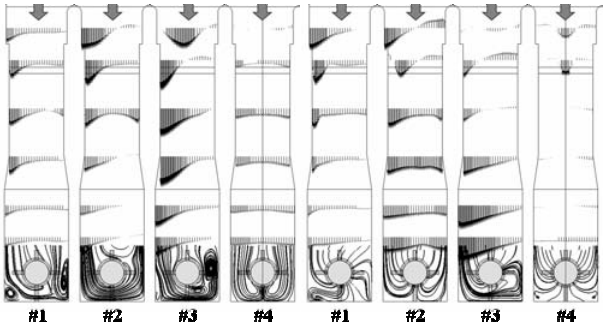

(a) H=100 mm (b) H=300 mm

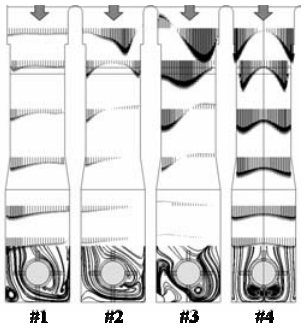

(c) H=500 mm

Fig. 14. Velocity profiles in the pump intake channels (with ADV).

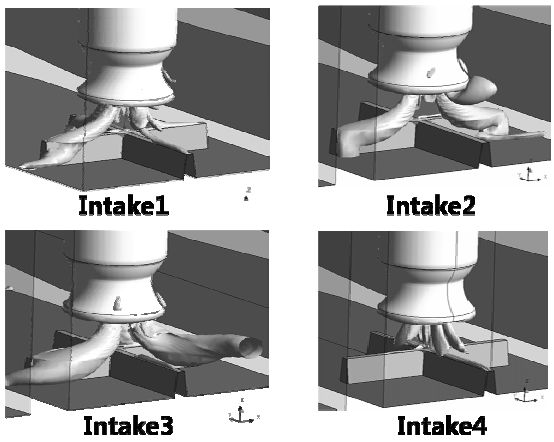

Fig. 15. Vortex core region in multi-intake pump sump model (with ADV).

Figs. 16 and 17 show that, at the bell-mouth inlet (H= 100mm), the vorticity distribution shows almost symmetric, and vorticity values at the height is considerably higher than those at the other heights regardless of the sampling direction. However, at the heights below the bell-mouth (H= 60mm and 80mm), very complicated vorticity distributions are found.

Below the height of bell-mouth inlet (H=60mm and 80mm), the locations of maximum vorticity value both in flow direction and channel width direction are inclined toward rear wall side (x/D_i=-1) (Fig. 16(b) and (c)) and right side wall (y/D_i=1) (Fig. 16(b) and (c)) in the all pump intakes except for the case of intake #4.

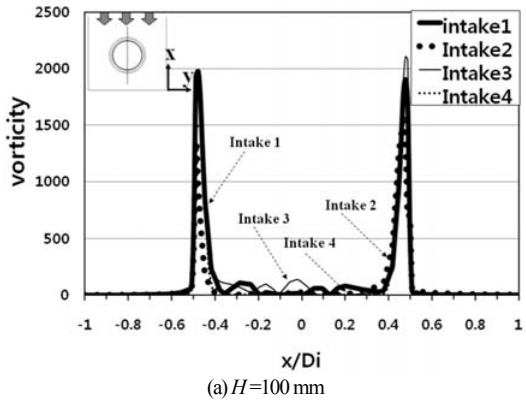

(a) H=100 mm

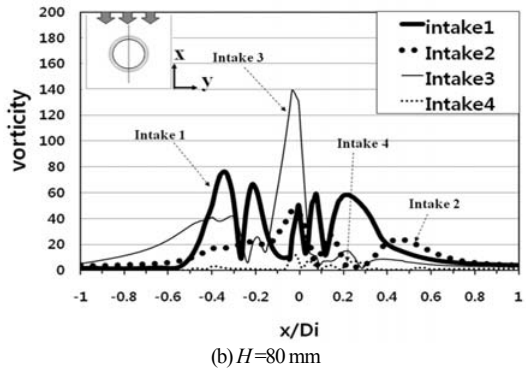

(b) H=80 mm

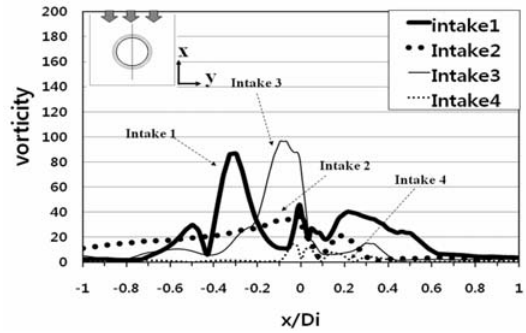

(c) H=60 mm

Fig. 16. Vorticity in flow direction (with ADV).

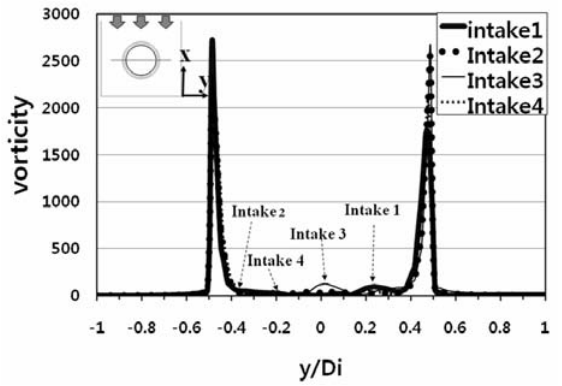

(a) H=100 mm

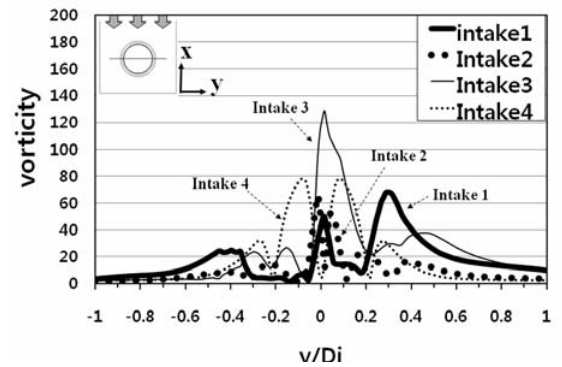

(b) H=80 mm

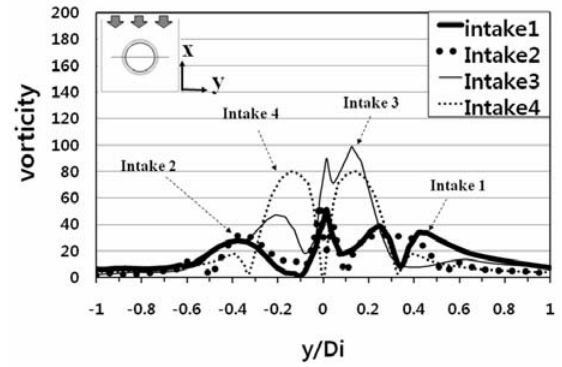

(c) H=60 mm

Fig. 17. Vorticity in direction of channel width (with ADV).

From the above examination for the vorticity distribution around the below bell-mouth inlet, it is clear that strong vortex occurrence in the pump intake #3 and the intermittent vortex occurrence in the other pump intakes (Table 2) are caused by the non-uniform distribution of maximum vorticity value around the bell-mouth inlet, and the non-uniform vorticity distribution is resulted from the unbalanced incoming flow in the pump intake channel.

Table 5 shows the summarized maximum and mean vorticity values in the multi-intake pump sump model. The data indicates that mean vorticity values of pump intake #3 under the height of bell-mouth inlet (H < 100mm) are about 1.5 times higher than those of the other pump intakes. Moreover, the difference between the maximum and mean vorticity values in all heights as well as in all pump sump intakes is considerable, which means that there exists possibility of considerable flow non-uniformity in the multi-intake pump sump.

3.4 Flow uniformity in a multi-intake pump sump

As the difference between the maximum and mean vorticity values shows considerable difference in Table 5, the flow uniformity is examined in the multi-intake pump sump model.

In order to examine quantitative flow uniformity of the incoming flow at each pump intake, flow uniformity S_v for the flow velocity in the pump intake channels is adopted using the concept of standard deviation as shown in Eq. (5).

$$S_v = \sqrt{\frac{\int (v-\bar{v})^2 dA}{A}} / \bar{v} \times 100 \quad [\%] \tag{5}$$

Table 5. Maximum & mean vorticity values of multi-pump intake sump model.

Distance from bottom wall in the pump sump model		Maximum & mean vorticity value			
		Sump 1	Sump 2	Sump 3	Sump 4
Channel width direction	60mm	51.3 (17.3)	55.3 (14.2)	98.8 (23.3)	80.4 (23.2)
	80mm	68.2 (17.3)	65.9 (9.8)	128.6 (22.4)	77.9 (17.2)
	90mm	85.3 (19.4)	70.2 (14.0)	126.1 (25.3)	56.6 (12.9)
	100mm	2671.7 {98.5} (118.5)	2504.5 {52.7} (114.0)	2626.9 {123.8} (119.1)	2126.7 {51.2} (121.0)
Flow direction	60mm	86.8 (20.6)	36.9 (13.7)	96.7 (15.1)	14.7 (2.1)
	80mm	76.0 (20.3)	46.3 (13.0)	123.9 (20.0)	11.4 (1.6)
	90mm	108.2 (23.8)	57.2 (15.9)	158.3 (25.4)	46.1 3.2)
	100mm	1976.4 {110.2} (123.4)	1539.1 {26.4} (85.3)	2108.0 {138.1} (129.3)	1575.8 {17.4} (90.1)

* (): mean vorticity value, ** { }:Second peak value

Table 6. Flow uniformity of y-z plane from rear wall in the pump sump model. (Unit : %)

Distance from rear wall in the pump sump model	Flow uniformity S_v on y-z plane			
	Sump 1	Sump 2	Sump 3	Sump 4
400mm	43.6	86.7	123.6	32.3
500mm	47.4	75.4	125.4	44.8
600mm	49.2	70.9	126.3	53.2
1100mm	47.1	77.1	125.4	62.9
1300mm	51.8	82.3	141.9	69.5
1500mm	60.4	103.3	156.6	80.9
Ave. value	49.9	82.6	133.2	57.3

where v denotes the local velocity and $\bar{v}$ means the area averaged velocity.

Table 6 shows the calculated flow uniformity using Eq. (5) for the incoming flow velocity in flow direction on the y-z cross-sectional plane in the pump intakes. Among the averaged values of the flow uniformity in the pump intake channels, pump intake #3 shows most high value of 133.2%, which means most high value of standard deviation of local velocity to the averaged velocity on the y-z cross-sectional plane of the flow channel. Therefore, most high vorticity and whirling flow is expected around the bell-mouth #3.

As a result, the reason of the highest value of flow uniformity at the inlet of pump intake #3 is caused by the non-uniform approaching velocity distribution at the inlet of the pump intake. The unbalanced flow patterns increases the value of flow uniformity S_v at the inlet of the pump intake channel. However, the value S_v becomes reduced as the flow goes closer to the region near bell-mouth by the flow rectification of the pump intake channel.

4. Conclusions

Flow uniformity in a multi-intake pump sump model is examined using experimental and numerical methods and the results are obtained as followings.

(1) The reason of the highest value of flow uniformity at the inlet of pump intakes #3 and #5 in the multi-intake pump sump with 7 pump intakes is caused by the non-uniform approaching velocity distribution at the inlet of the pump intake. The unbalanced flow patterns increases the value of flow uniformity S_v at the inlet of the pump intake channel.

(2) One of the most important factors for the pump station design is to consider the flow patterns at the upstream region of pump intake inlet in the forebay diffusing area. The large expanding angle at the forebay diffusing area may cause unstable fluctuating flow supply to pump intake channels.

(3) Submerged vortex intensity in the vicinity of side walls is higher than those both near rear wall and near the upstream region of the bell mouth. However, the strong submerged vortex can be successfully suppressed by the installation of anti-submerged vortex device on the bottom of pump intake channel beneath the bell mouth.

(4) Vorticity around the bell-mouth shows higher value in the multi-intake pump sump in comparison with that in the single-intake pump sump because of the higher non-uniform approaching velocity in the multi-intake pump sump channel.

Nomenclature

A : Cross-sectional area of pump intake channel
AVD : Anti-submerged vortex device
D_i : Inner diameter of bell-mouth
dA : Local cross-sectional area of pump intake channel
F_r : Froude number ($=\frac{V}{\sqrt{gL}}$)
g : Acceleration of gravity
H : Height from pump intake bottom wall
L : Reference length
L_m : Reference length for model
L_p : Reference length for prototype
Q_m : Flow rate for model
Q_p : Flow rate for prototype
S_v : Flow uniformity
v : Local flow velocity
$\bar{v}$: Area averaged incident flow velocity
V_m : Flow velocity for model
V_p : Flow velocity for prototype
X : Distance in flow direction at benchmarking pump

sump model
x : Distance in flow direction
Y : Distance in direction of channel width at benchmarking pump sump model
y : Distance in direction of channel width
Z : Distance in flow vertical direction at benchmarking pump sump model
z : Distance in flow vertical direction

References

[1] M. Padmanabhan and G. E. Hecker, Scale Effects in Pump Models, ASCE J. Hydraulic Engineering, 110 (11) (1984) 1540-1556.

[2] V. P. Rajendran, S. G. Constantinescu and V. C. Patel, Experiments on Flow in Model Water-pump Intake Sump to Validate a Numerical Model, Proc. of ASME Fluids Engineering Division Summer Meeting, (1998) FEDSM98-5098.

[3] K. Kamemoto, K. Suzuki and T. Mugiyama, An Experimental Study on Similarity of Vortex Formation Characteristics in Two Different Scale Models of Pump Sump, Proc. of the 9th Asian International Conference on Fluid Machinery, (2007) No. AICFM9-235.

[4] T. Nagahara, T. Sato and T. Okamura, Measurement of the Flow around the Submerged Vortex Cavitation in a Pump Intake by Means of PIV, Proc. of Fifth International Symposium on Cavitation, (2003) Cav03-OS-6-011.

[5] Y. H. Lee, Establishment of Design Guideline for the Pump Intake Shape using the Result of Model Test, R&D Report, K-water (in Korean) (2004).

[6] Turbomachinery Society of Japan, Standard Method for Model Testing the Performance of a Pump Sump, TSJ S002, (2005).

[7] R. B. Abernethy, R. P. Benedict and R. B. Dowdell, ASME Measurement Uncertainty, ASME J. Fluids Eng. 107 (1985) 161-164.

[8] Hydraulic Institute, Pump Intake Design, ANSI/HI 9.8-1998, (1998).

[9] ANSYS-CFX Documentation Ver. 11, ANSYS Inc., (2007).

[10] F. R. Menter, M. Kuntz and R. Langtry, Ten Years of Industrial Experience with the SST Turbulence Model, Proc. of the Fourth International Symposium on Turbulence, Heat and Mass Transfer, Begell House, Redding, CT, (2003).

Jong-Woong Choi received his B.E. and M.E. degrees in Mechanical Engineering from Korea Maritime University, Korea in 2001 and 2003, respectively. Mr. Choi is currently a doctorate student in the Department of Mechanical Engineering, Graduate School, Korea Maritime University. His research interest includes fluid machinery, ocean energy, wind energy.

Young-Do Choi received his B.E. and M.E. degrees in Mechanical Engineering from Korea Maritime University, Korea in 1996 and 1998, respectively. He received his Ph.D. in Engineering from the Yokohama National University, Japan in 2003. Dr. Choi is currently a professor at the Department of Mechanical Engineering, Mokpo National University, Korea. His research interests include fluid machinery, ocean energy, wind power, small hydro power.

Chang-Goo Kim received his B.E. and M.E. degrees in Mechanical Engineering from Korea Maritime University, Korea in 2007 and 2009, respectively. Mr. Kim is currently a doctorate student in the Department of Mechanical Engineering, Graduate School, Korea Maritime University. His research interest includes fluid machinery, ocean energy.

Young-Ho Lee received his B.E. and M.E. degrees from Korea Maritime University, Korea. He received his Ph.D. in Engineering from the University of Tokyo, Japan. Dr. Lee is currently a Professor at the Division of Mechanical and Information Engineering, Korea Maritime University. His research interests include fluid machinery, ocean energy, wind energy, small hydro power, PIV, and CFD.